Identification of new dasatinib analogues targeting mutated BCR-ABL1: Virtual screening, molecular docking, and dynamics simulations studies

Mohammad Jahoor Alam

j.alam@uoh.edu.sa

University of Ha'il

Arshad Jamal

University of Ha'il

Shaik Daria Hussain

University of Ha'il

Shahzaib Ahamad

International Centre for Genetic Engineering and Biotechnology

Dinesh Gupta

International Centre for Genetic Engineering and Biotechnology

Ashanul Haque

University of Ha'il

Research Article

Keywords: ABL1, Dasatinib derivatives, Cancer, molecular docking, MD Simulations

Posted Date: June 12th, 2025

DOI: https://doi.org/10.21203/rs.3.rs-6855109/v1

Additional Declarations: No competing interests reported.

Identification of new dasatinib analogues targeting mutated BCR-ABL1: Virtual screening, molecular docking, and dynamics simulations studies

Mohammad Jahoor Alam[1*], Arshad Jamal,[1] Shaik Daria Hussain,[2] Shahzaib Ahamad[3], Dinesh Gupta[3] , and Ashanul Haque[4]

[1] Department of Biology, College of Science, University of Hail, Kingdom of Saudi Arabia.

[2] Department of Physiotherapy, College of Applied Medical Sciences, University of Ha'il, Ha'il 2440, Saudi Arabia.

[3] Translational Bioinformatics Group, International Centre for Genetic Engineering and Biotechnology (ICGEB), Aruna Asaf Ali Marg 110067 New Delhi, India

[4] Department of Chemistry, College of Science, University of Hail, Kingdom of Saudi Arabia.

Abstract

Drug resistance is a significant challenge in cancer chemotherapy and accounts for a large number of cancer-related deaths globally. One of the well-identified and characterized mechanisms of drug resistance is the presence of BCR-ABL1 mutations in chronic myeloid leukaemia (CML). These mutations are associated with resistance to FDA-approved first-line tyrosine kinase inhibitors (TKI) such as imatinib, dasatinib, and nilotinib. The present work reports virtual screening, molecular docking, and dynamics simulation results of new-generation anticancer agents. To this end, we performed a three-tier virtual screening to identify three new Dasatinib analogues (45375848, 88575518, and 23589024) selected based on their docking score and ADMET profiles. To understand the affinity, dynamics, and stability of the ligand-protein complexes, a 500 ns MD simulation was carried out and compared. Density functional theory (DFT) at B3LYP was carried out. The three compounds that were identified all contained the common fragment N-(2-chloro-6-methylphenyl)-2-(methylamino)thiazole-5-carboxamide. Docking results predicted that the identified compounds have higher affinity than the dasatinib towards ABL1. The interacting residues were the same as those of the various dasatinib analogues. MD simulations further complemented the docking results, showing stabilization of the ABL1 receptor in the presence of ligands. High drug-likeness and acceptable pharmacokinetic profile warranties the drug-like behaviour of the compounds. This study highlights promising ABL1 inhibitors, laying the groundwork for further in vitro and in vivo investigations.

***Keywords*:** ABL1, Dasatinib derivatives, Cancer, molecular docking, MD Simulations

Introduction

Among a number of non-communicable disease-related deaths, cancer has been a major killer for ages. According to the report, over 20 million new cases of cancer were diagnosed worldwide, resulting in 9.7 million deaths [1]. While there has been significant progress made in oncological diagnostics and therapeutics, drug resistance continues to be the principal limiting factor to achieving cures in patients with cancer [2]. Various approaches have been suggested to overcome the problem of resistance (e.g., the use of a combination of drugs, their varying doses, etc.). One key and successful approach is pursuing the oncogene targets that undergo mutation and reduce the effectiveness of a drug. One such example is the BCR–ABL1 protein mutation, which leads to resistance against tyrosine kinase inhibitors (TKIs). ABL1 is a non-receptor tyrosine-protein kinase involved in critical cellular processes, including cytoskeleton remodelling, cell motility, adhesion, receptor endocytosis, autophagy, DNA damage repair, and apoptosis [3-5]. ABL1 translocates to the nucleus and plays a significant role in DNA damage response and apoptosis [6]. It phosphorylates multiple DNA repair mediators, including DDB1, DDB2, ERCC3, ERCC6, RAD9A, RAD51, RAD52, and WRN, which facilitate the repair of damaged DNA [7] When DNA damage is irreparable, ABL1 activates pro-apoptotic pathways, such as by phosphorylating TP73, a key regulator of DNA damage-induced apoptosis [8]. ABL1 is a critical target in cancer treatment due to its role in oncogenic signalling, particularly in chronic myeloid leukaemia (CML) [9,10]. While imatinib effectively treats early-stage CML by inhibiting ABL kinase activity, resistance due to point mutations in the ABL domain remains a major challenge [11,12]. Dasatinib, a second-generation tyrosine kinase inhibitor, has shown potent activity against both wild-type and imatinib-resistant BCR-ABL mutants, including those resistant to other therapies [13-15]. It has been demonstrated that dasatinib can inhibit multiple kinases, including Bcr-Abl and Src family members. Despite its high and broad effectiveness, Yeung and coworkers [15] noted the relapse of BCR-ABL1-like ALL in the patient after nine months. Molecular analysis revealed a T315I mutation in the ABL1 kinase domain, leading to the disrupted binding of dasatinib and similar TKIs. Besides its poor selectivity, anaemia, pulmonary oedema, and heart function complications remain a major concern [16]. One way to alleviate this problem is to design new molecular entities that can evade the resistance mechanism.

In the present work, we applied a three-tier virtual screening approach and screened over 7,500 dasatinib-like molecules available in the PubChem database. To this end, we searched two halves of dasatinib separately, identifying the top three compounds (45375848, 88575518, and 23589024). This is followed by induced fit docking (IFD) to explore the flexibility of the ABL1 kinase binding pocket and to confirm the binding modes of the selected compounds. We analyzed drug-likeness and ADMET (absorption, distribution, metabolism, excretion, and toxicity) profiles to assess their pharmacokinetic properties, ensuring their suitability for drug development. Finally, molecular dynamics (MD) simulations

at 500 ns were carried out to evaluate the stability and dynamic behaviour of the protein-ligand complexes. The simulations included a detailed analysis of root-mean-square deviation (RMSD), root-mean-square fluctuation (RMSF), secondary structure elements (SSE), hydrogen bond interactions, and interaction fractions between the protein and ligands.

Material and method

The workflow adopted in this work is depicted in **Fig. 1**. Fragments AP and Tz were (**Fig. S1**, *supporting information*) used to screen the PubChem database. The identified compounds were scored based on XP GlideScore. Following their ADMET studies, MD simulation and DFT studies were carried out to understand dynamic behaviour and structural features of the compounds.

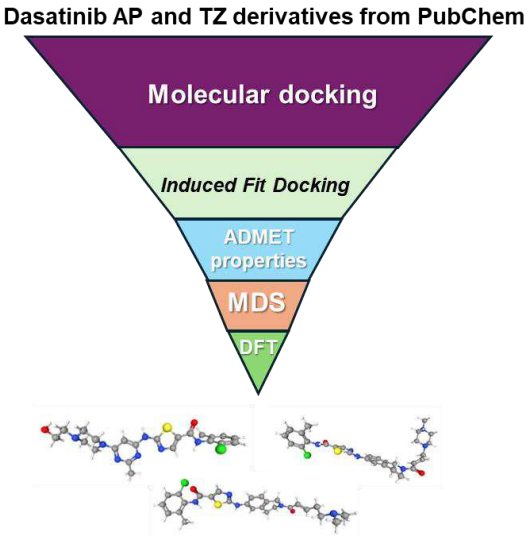

Figure 1: The workflow adopted in this work.

Computer configuration

All computational studies were conducted on a Dell Precision 7920 workstation with 20 Intel Xeon Silver cores, 128 GB of RAM, and an NVIDIA Quadro RTX 8000 GPU with 32 GB of dedicated memory.

Dataset collection and protein preparation

Dasatinib derivatives were retrieved from the PubChem database for computational modeling [17]. A total of 653 AP scaffold compounds and 2,537 substructures, along with 79 TZ similarity scaffolds and 3,521 substructures, were selected. The dataset was downloaded in SDF format for further analysis. Dasatinib (BMS-354825, identified as 1NI (Co-crystal ligand)) was chosen as the reference ligand due to its well-characterized protein interactions and therapeutic significance. The human Tyrosine-protein kinase ABL1 (UniProt ID: P00519) was used as the target protein. The crystal structure of ABL1 bound to Dasatinib

(PDB ID: 2GQG) was obtained from the Protein Data Bank (PDB) and served as the template for computational studies (https://www.rcsb.org/) [18].

Molecular Docking

Molecular docking was performed using Glide (Version 12.0.1, Schrödinger, 2024). Protein and ligand structures were prepared using Protein Preparation Wizard and LigPrep, ensuring proper geometry and protonation states. A receptor grid was generated to define the ABL1 active site for docking [19]. Docking was conducted in three modes: High-Throughput Virtual Screening (HTVS) for rapid screening, Standard Precision (SP) for balanced accuracy, and Extra Precision (XP) for detailed interaction analysis. XP GlideScore (GScore) evaluated binding affinities, providing insights into ligand-receptor interactions. The OPLS3e force field was applied to ensure accuracy. Virtual screening was automated using the Schrödinger suite, with default parameters optimizing ligand evaluation based on GlideScore [20,21].

Induced Fit Docking (IFD)

IFD was performed using the Schrödinger Suite. Protein Preparation Wizard was used for bond correction, protonation assignment, hydrogen addition, and energy minimization with the OPLS3e force field. A 20 Å receptor grid was generated in Glide, targeting active site residues. Glide XP mode performed initial docking, selecting the top three ligands based on GlideScores [22]. The Prime module refined protein-ligand interactions by introducing side-chain flexibility and localized backbone adjustments. Binding poses were analyzed for hydrogen bonds, hydrophobic contacts, and salt bridges, ensuring optimal binding affinity [23].

ADMET properties evaluation

To identify candidates with favourable pharmacokinetics and minimized risk of adverse effects, ADMET (Absorption, Distribution, Metabolism, Excretion, and Toxicity) parameters were determined using the QikProp (Schrödinger Suite) (Schrödinger Release 2024-4: QikProp, Schrödinger, LLC, New York, NY, 2024). Key assessments included Lipinski's Rule of Five for drug-likeness, QPlog Po/w for hydrophilic-lipophilic balance, QPlogS for aqueous solubility, QPP Caco-2 and MDCK permeability for intestinal and blood-brain barrier simulations, QPlog HERG for cardiotoxicity risk, polar surface area (PSA) for membrane permeability, and hydrogen bond donors/acceptors for interaction potential [24].

Molecular Dynamics (MD) Simulation

MD simulations were performed using Desmond (Schrödinger) to evaluate the stability and dynamic behaviour of native ABL1 kinase and its complexes with Dasatinib, ABL1-45375848, ABL1-88575518, and ABL1-23589024. The System Builder tool prepared the complexes, which were solvated in a TIP3P

water box (10 Å buffer), neutralized with counterions, and supplemented with 0.15 M NaCl to simulate physiological conditions [25]. The OPLS_2005 force field was applied, followed by energy minimization using the steepest descent algorithm. The system was equilibrated at 300 K and 1 atm before a 500 ns production run with a 2-fs time-step. Trajectory analysis included RMSD for structural stability, RMSF for residue flexibility, and protein-ligand interaction analysis to identify key stabilizing forces [26].

Results and discussion

Molecular docking

A fragment-based search strategy using AP and Tz scaffolds led to the identification of 3,190 and 3600 compounds available in the PubChem database. These compounds were downloaded in .sdf format and used for further studies. Dasatinib complex with ABL1 kinase (PDB ID: 2GQG) was used as a reference [18]. Among the 6,790 Dasatinib derivatives, the top three compounds, namely **45375848** (N-(2-chloro-6-methylphenyl)-2-((2-(4-(4-methylpiperazin-1-yl)but-2-enoyl)-1,2,3,4-tetrahydroisoquinolin-7-yl)amino) thiazole-5-carboxamide), **45375848** (N-(2-chloro-6-methylphenyl)-2-((2-(5-(dimethylamino)pent-2-enoyl)-1,2,3,4 tetrahydroisoquinolin-7-yl)amino)thiazole-5-carboxamide) and **23589024** (2-((6-(5-(1H-imidazol-1-yl)pentyl)pyridin-2-yl)amino)-N-(2-chloro-6-methylphenyl)thiazole-5-carboxamide were selected for further studies (**Fig. 2** and **Table 1**). It is to be noted that the top three filtered compounds bear N-(2-chloro-6-methylphenyl)-2-(methylamino)thiazole-5-carboxamide fragments in common.

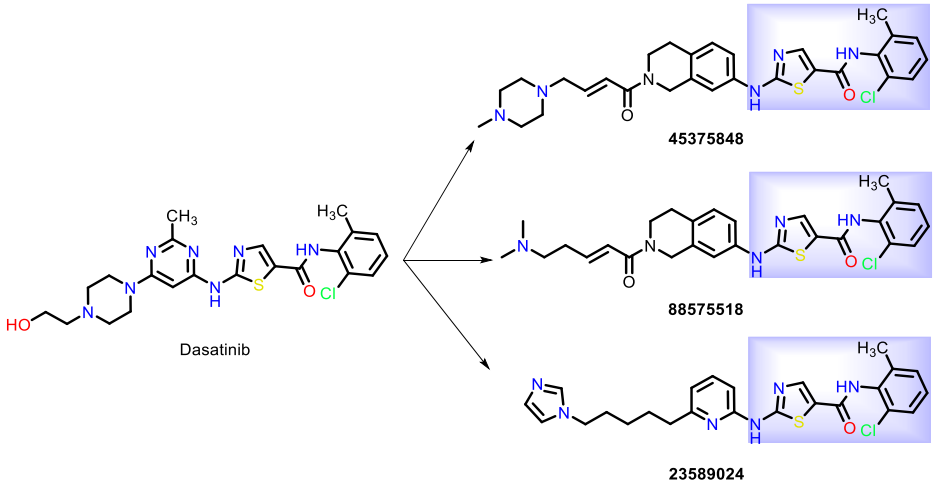

Figure 2: Chemical structures of dasatinib, 45375848, 45375848, and 23589024**.** Highlighted areas show common fragments.

The docking study predicted that the reference inhibitor dasatinib interacted with the ABL1, resulting in XP GlideScore = –10.74 kcal/mol **(Figure 3a)**. It formed an H-bond with the Met318 and Asp325 residues; H-bond with the former (Met318) is crucial for activity against both native and mutated BCR-ABL kinases [27]. The N-atom of thiazole of dasatinib served as the acceptor, while ethan-1-ol served as the donor donor fragments. This interaction was found to be shared in all the identified

compounds. A significant increase in docking score was noted for the compound **45375848** (XP GlideScore = –14.80 kcal/mol). This compound was also found to form H-bond with residues including Gln252 and Met318 (**Figure 3b**). This compound in which the 2-(4-(2-methyl-6-(amino) pyrimidine-4-yl) piperazine-1-yl)ethan-1-ol fragment is replaced by a bulkier 7-amino-3,4-dihydroisoquinolin-2(1H)-yl)-4-(4-methylpiperazin-1-yl)but-2-en-1-one assisted the ligand in interacting with receptor via other non-conventional H-bonds. Almost a similar score (XP GlideScore = –14.63 kcal/mol) was found for structurally similar compound **88575518**, which interacted through three H-bonds involving Glu248, Thr319, and Asp381 residues (**Figure 3c**). The terminal N-methyl piperazine fragment was replaced in this compound by N, N-dimethyl group. Such interaction is similar to that shown for ponatinib with BCR-ABL^{T315I}, which forms an H-bond with Asp381 [28]. Albeit a lower score (XP GlideScore = –13.79 kcal/mol) and two H-bonds (Met318 and Asn322) were predicted for the compound **23589024**. In this compound, the amino group of 2-amino pyridine formed an H-bond with Met318 (**Figure 3d**).

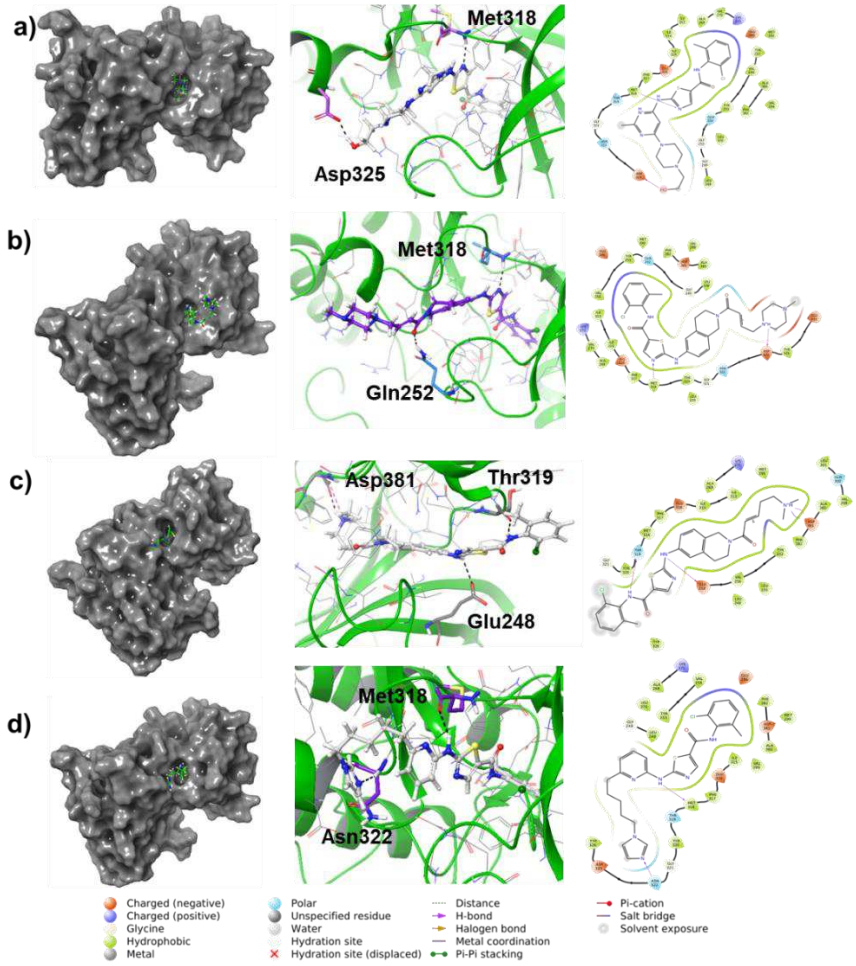

Figure 3: Molecular docking studies results of (a) dasatinib, (b) 45375848, (c) 88575518, and (d) 23589024 with Abl1 kinase.

Pharmacokinetic profiles

In drug development research, predicting pharmacokinetic properties using in-silico tools has become indispensable [29]. Not only does it save time, but it also reduces overall costs, which are key criteria for the pharmaceutical industry. Herein we estimated various features, including the SASA (solvent-accessible surface area), FOSA (hydrophobic surface area), FISA (hydrophilic surface area), PISA (polar surface area), WPSA (weakly polar surface area), volume, donorHB (hydrogen bond donors), and accptHB (hydrogen bond acceptors) and others. These features are predicted using the XP Glide Score and given in (**Table 1** and **Table 2**). The results indicate dasatinib and **23589024** exhibited moderate CNS activity (-1), while 45375848 and 88575518 were predicted to be active (+1). While the reference dasatnib (MW = 488.01) and **23589024** (MW = 481.01) showed MW < 500, the other two compounds had slightly higher MW, which is acceptable for a drug candidate [30]. The average number of HBD and HBA was found to be 2 and 7.5-11.5, respectively. Solubility profiles like QPlogS (–6.26 to –7.80) and CIQP logS (–5.10 to –7.25) were close to the recommended value. We also noted that QPPCaco, which is the predicted apparent Caco-2 cell permeability, was highest for **23589024** (1054.936 nm/sec) followed by **88575518** (239.083 nm/sec), dasatinib (147.391nm/sec) and **45375848** (34.76 nm/sec). Except for **45375848** (HOA = 64.577%), all compounds showed high human oral absorption (HOA = 83.82-100%). Lower QPPCaco and HOA could be attributed to the high C-content in the molecule. The predicted binding to human serum albumin QplogKhsa was 0.168 to 0.797, which is within the recommended value (-1.5 to +1.5).

Table 1: The pharmacokinetic and physicochemical (ADME) properties determined using XP GlideScore.

Title	CNS	Mol MW	Dipole	SASA	FOSA	FISA	PISA	WPSA	Volume	DonorHB	AccptHB	XP GScore
Dasatinib	-1	488.01	1.97	843.52	381.89	129.11	230.65	101.86	1484.99	3	10.7	-10.74
45375848	1	565.13	7.18	970.98	456.18	131.66	297.78	85.35	1744.71	2	11.5	-14.80
88575518	1	524.07	9.50	932.08	419.18	106.95	308.73	97.21	1654.97	2	9.5	-14.63
23589024	-2	481.01	6.53	859.14	235.95	102.57	421.11	99.49	1512.55	2	7.5	-13.79

Table 2: The ADMET properties of compounds determined using XP GlideScore.

Title	QPpolrz	QPlog PC16	QPlog Poct	QPlog Pw	QPlog Po/w	QPlogS	CIQP logS	QPlog HERG	QPP Caco	QPlog BB	QPP MDCK	QPlog Kp	QPlog Khsa	HOA
Dasatinib	50.984	16.333	27.315	17.621	3.085	-5.676	-4.859	-7.464	147.391	-0.756	249.711	-4.477	0.168	83.823
45375848	62.019	19.228	30.493	17.72	3.929	-6.26	-5.103	-8.905	34.76	-0.537	47.07	-6.35	0.666	64.577
88575518	57.89	18.309	28.397	15.346	4.97	-7.445	-6.029	-8.165	239.083	-0.635	397.211	-3.698	0.797	85.661
23589024	51.979	17.55	24.88	13.495	5.621	-7.807	-7.257	-7.719	1054.936	-1.038	1838.619	-0.966	0.744	100

Molecular dynamics simulations

The stability and dynamic behaviour of the complexes provide critical insights into the potential efficacy of a proposed compound [31]. Such studies are essential for drug optimization against ABL1 kinase. Herein, we performed and compared the MD simulation results of native ABL1 kinase and ABL1-45375848, ABL1-88575518, and ABL1-23589024 complexes.

RMSD analysis

Fig. 4 presents the RMSD profiles for the protein and its complexes during the 500 ns simulations studies. The RMSD of the Cα atoms was calculated to assess the global structural deviations of the systems relative to their initial conformations. This metric reflects the overall stability and equilibration of the protein-ligand complexes during the simulation [32]. All the study complexes reached equilibrium within the initial 50 ns of the trajectory. The native ABL1 protein exhibited significant fluctuations between 150 and 425 ns, suggesting higher flexibility or potential conformational changes. However, the RMSD stabilized in the last 75 ns of the trajectory, indicating that the system achieved a more stable configuration during this period.

The ABL1-dasatinib complex exhibited RMSD in the range of 1.8–5.2 Å. Initially, the complex displayed a stable trajectory; however, increased fluctuations were observed between 300 and 500 ns, with the average RMSD reaching 2.97 Å. This increase in fluctuation suggests a degree of conformational flexibility, potentially influenced by ligand binding or protein adjustments during the simulation [33]. In contrast, the ABL1-45375848 complex demonstrated a relatively smooth RMSD trajectory, with only a slight increase in fluctuation between 480 and 500 ns, where the RMSD reached 3.8 Å. Despite this, the average RMSD remained stable at 2.97 Å, indicating that the ABL1-45375848 complex maintained a stable configuration during the simulation, suggesting favourable interactions between the ligand and the protein binding site.

The ABL1-88575518 complex exhibited a particularly stable RMSD profile, with minimal fluctuations throughout the entire simulation. The only significant deviation was observed between 195 and 205 ns, where the RMSD reached a peak of 3.8 Å. The overall RMSD for this complex remained low, with an average of 2.53 Å, indicating a stable binding interaction and minimal conformational changes during the MD simulation. Lastly, the ABL1-23589024 complex showed small RMSD peaks at 25 ns and 65 ns, where the fluctuation reached a maximum of 3.2 Å. After these early fluctuations, the trajectory became stable, with the protein-ligand complex maintaining a smooth and consistent behaviour for the remainder of the simulation. The average RMSD for the ABL1-23589024 complex was 2.31 Å, further supporting its stable binding and minimal structural deviation. The MD simulations revealed that all complexes, including ABL1-Dasatinib and the novel compounds, demonstrated relative stability during the 500

nanosecond trajectories. However, the minimal fluctuations and low RMSD values of ABL1-45375848, ABL1-88575518, and ABL1-23589024 suggest that these compounds could form stable interactions with ABL1, potentially indicating their suitability as effective inhibitors.

Following this, we also estimated the ligand RMSD values (**Fig. 4b**). The average ligand RMSD values for the complexes with dasatinib, 45375848, 88575518, and 23589024, were calculated to be 1.36 Å, 3.66 Å, 3.41 Å, and 2.83 Å, respectively (**Supplementary Table S1**). The ligand RMSD for Dasatinib indicated a highly stable binding, as reflected by its low average RMSD of 1.36 Å. This stability suggests a consistent ligand positioning within the ABL1 binding pocket, indicative of strong and enduring interactions with key residues. In contrast, the RMSD values particularly for 45375848 (RMSD = 3.66 Å) and 88575518 (RMSD = 3.41 Å). The ligands exhibit moderate flexibility within the binding site, likely due to transient interactions and structural adjustments during the simulation. Compared to these two ligands, compound 23589024 exhibited relatively lower (RMSD = 2.83 Å) value, implying better stability.

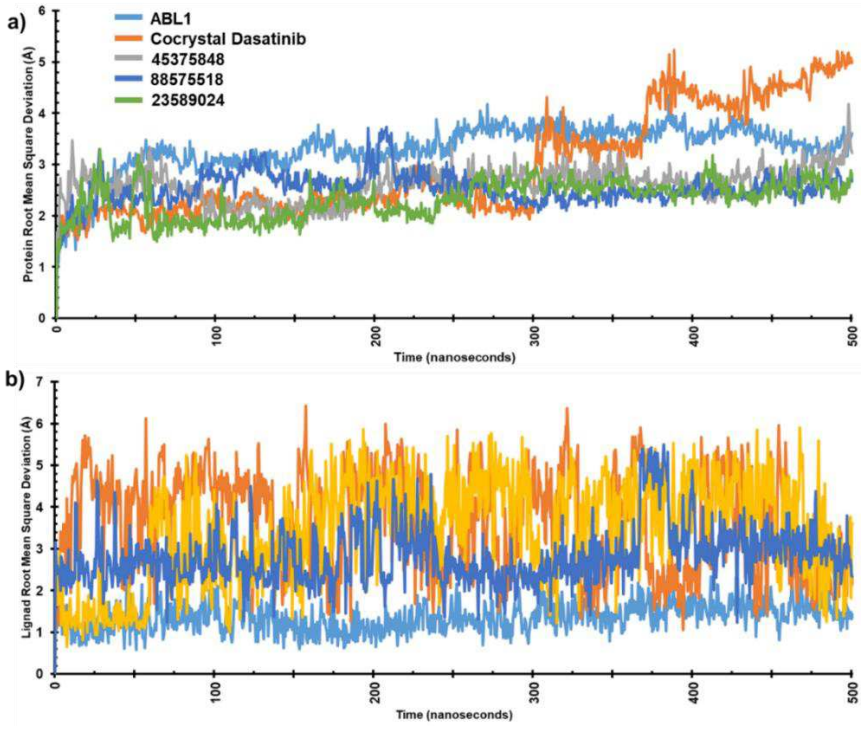

Figure 4: (a) Protein and (b) ligand RMSD vs time plots obtained by MD simulation at 500 ns.

RMSF analysis

RMSF reflects the deviation of atoms or residues from their average positions over the simulation time, offering insights into structural dynamics and flexibility RMSF was analyzed to understand local residue flexibility (Protein-RMSF) and atom-wise fluctuations in Ligand-protein complex during the MD simulation

[34]. For the native ABL1, the average RMSF was calculated to be 1.40 Å. Notable regions of flexibility were observed, particularly in the Gly251–Glu255 region, where fluctuations peaked at 5.8 Å, suggesting increased flexibility in this loop or surface-exposed area. The ABL1-Dasatinib complex exhibited an average RMSF of 1.51 Å. This complex formed hydrogen bonds with Met318 and Asp325 in the active site (**Fig. 5**). Higher flexibility was observed in the Gly227–Trp235 region, while the rest of the structure demonstrated stable behaviour with minimal fluctuations, indicating that ligand binding stabilized most regions of the protein while allowing localized flexibility.

For the ABL1-45375848 complex, the RMSF analysis revealed a highly stable profile with no significant peaks in flexibility across the protein. The average RMSF value was 1.22 Å, demonstrating that ligand binding contributed to the overall stabilization of the protein structure during the simulation. The ABL1-88575518 complex showed minor fluctuations, with a peak in the Leu387–Asp391 region where RMSF reached only 3.5 Å. Despite this localized movement, the overall protein exhibited stability with an average RMSF of 1.34 Å, underscoring its potential as a stable inhibitor. Finally, the ABL1-23589024 complex exhibited slightly higher flexibility in the Gly251–Glu255 region, similar to the native protein. The peak RMSF value in this region was 3.8 Å, while the rest of the structure remained stable. The average RMSF for the complex was calculated as 1.29 Å, suggesting a balanced dynamic behaviour of the protein upon ligand binding. The RMSF analysis highlighted the stabilizing effect of ligands on the ABL1 protein, with each complex exhibiting unique patterns of flexibility. The localized fluctuations in specific regions suggest that ligand binding may allow dynamic adjustments critical for effective binding and inhibition. These results provide key insights into the interaction dynamics and potential efficacy of the inhibitors.

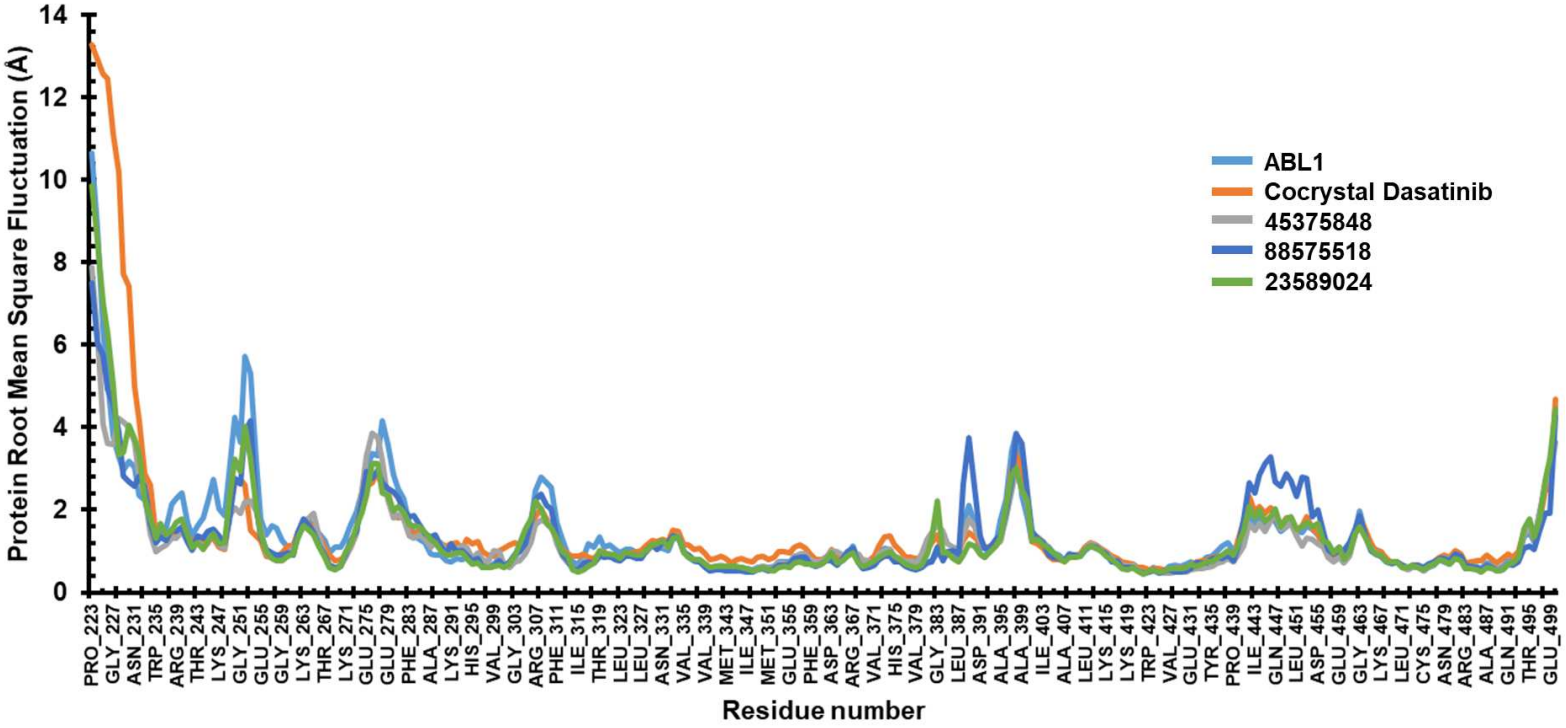

Figure 5: Protein RMSF vs residues number plots obtained by MD simulation at 500 ns.

Secondary Structure Elements (SSEs) analysis

The SSE of the ABL1 protein, including α-helices (depicted in orange) and β-strands (represented in sky blue), were analyzed throughout the simulation. The upper plot displays the distribution of SSEs across the residue index throughout the protein structure. The middle plot summarises the SSE composition for each trajectory frame during the simulation. In contrast, the lower plot tracks the SSE assignment for each residue over the 500 ns simulation period. For the ABL1 protein, the secondary structure composition was found to be 30.07% helix, 14.58% strand, and 44.65% total SSE (**Fig. 6a** and **Fig. S3**). When the ABL1 protein formed a complex with the co-crystallized ligand dasatinib, the secondary structure percentages changed to 30.01% helix, 15.03% strand, and 45.04% total SSE (**Fig. 6b**). The ABL1 complex with compound 45375848 exhibited 30.15% helix, 14.56% strand, and 44.71% total SSE (**Fig. 6c**). In contrast, the ABL1 complex with compound 88575518 displayed 28.44% helix, 16.43% strand, and 44.86% total SSE, while the ABL1 complex with compound 23589024 showed 29.83% helix, 14.76% strand, and 44.59% total SSE (**Fig. 6d-e**). The analysis of secondary structure elements across the various ABL1 complexes reveals subtle but notable differences in SSE composition when interacting with different compounds. The slight variations in the percentage of helices and strands could reflect how each compound influences the structural stability and dynamics of the protein, potentially impacting its function and binding properties. These results suggest that ligand binding can modulate the protein's conformational state, which may affect its activity in therapeutic contexts.

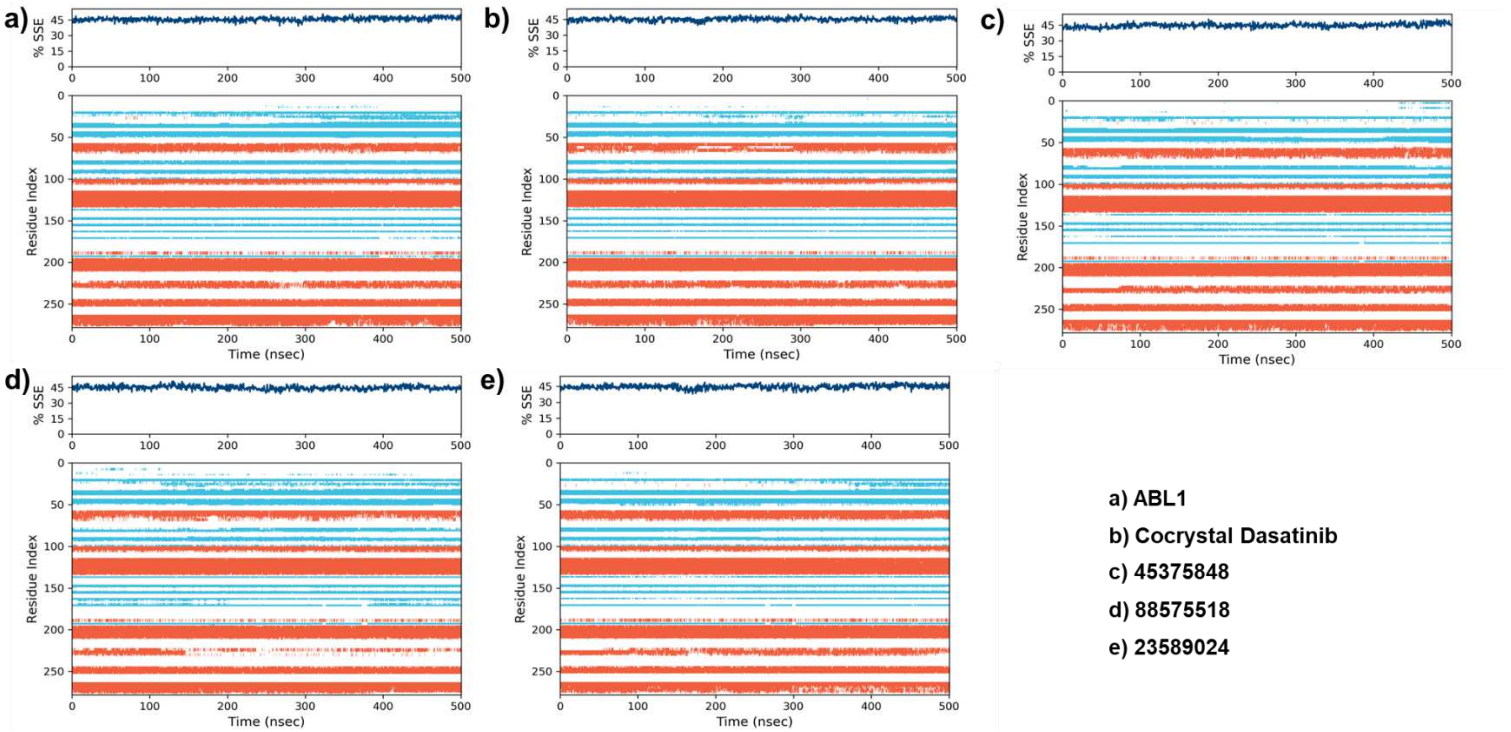

Figure 6: The secondary structure elements and residue index plot of the 500 ns MD simulation of native Abl1 kinase with four ligands—co-crystallized ligand Dasatinib and its derivatives 45375848, 88575518, and 23589024—were analyzed.

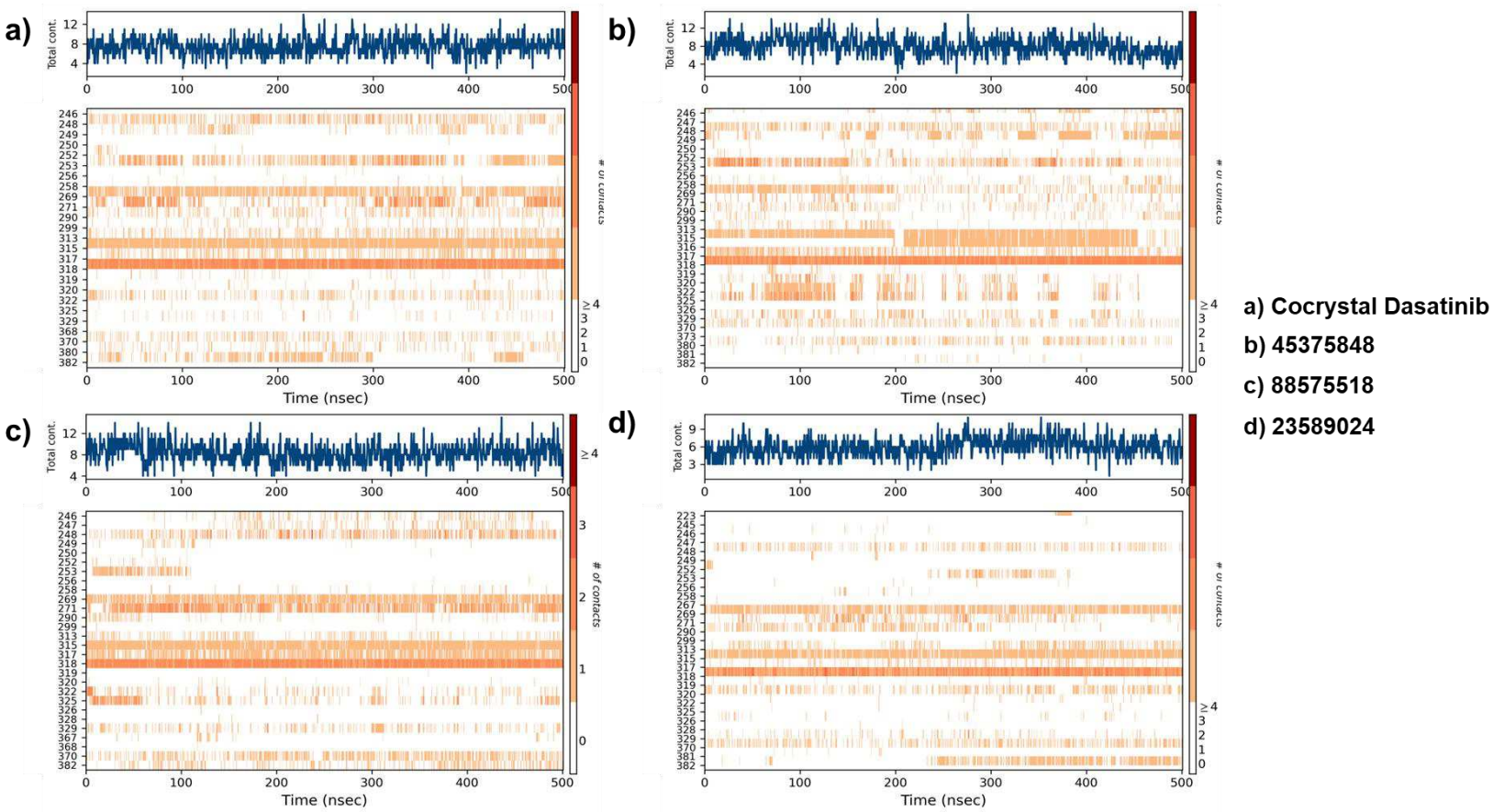

Figure 7: Timeline illustrating the interactions (H-bonds, Hydrophobic, Ionic, Water bridges) between Abl1 kinase and four ligands (dasatinib, 45375848, 88575518, and 23589024). The top panel shows the total number of contacts made by the protein with the ligand throughout the trajectory, while the bottom panel highlights the residues interacting with the ligand in each frame. Residues making multiple contacts are shown in a darker shade of orange, as indicated by the scale.

Fig. 7 depicts the timeline plot highlighting the dynamic interactions and contacts (including hydrogen bonds, hydrophobic interactions, ionic bonds, and water bridges) between the protein and the ligand throughout the simulation. The top panel depicts the total number of interactions over time, while the bottom panel highlights the specific residues involved in ligand binding during each trajectory frame [35]. Residues that participate in multiple interactions with the ligand are represented with a darker orange shade, as shown in the color scale on the right, emphasizing the key residues involved in stabilizing the protein-ligand complex. In particular, the ABL1 complex with the co-crystallized dasatinib consistently interacted with residues such as His246, Gln252, Glu258, Ala269, Ile313, Phe317, Met318, and Phe382, which regularly made contact with the ligand (**Fig. 7a**). Similarly, the ABL1 complex with the 45375848-ligand demonstrated consistent interactions with Lys247, Gln252, Ala269, Ile313, Glu316, Phe317, Met318, and Asn322 (**Fig. 7b**). The ABL1 complex with the 88575518-ligand maintained regular contacts with Leu248, Ala269, Lys271, Ile313, Ile315, Glu316, Phe317, Met318, and Val371 (**Fig 7c**). Lastly, the ABL1-23589024 complex displayed stable interactions with Lys247, Thr267, Lys271, Met290, Ile313, Phe317, Met318, and Glu329 (**Fig. 7d**). These results reveal that specific residues play a crucial role in stabilizing the ligand-protein complex. The consistent interaction of these residues suggests their importance in maintaining the integrity and specificity of the binding, which may have implications for the design of more effective inhibitors targeting the ABL1 protein.

The Desmond simulation results for ligand RMSD, rGyr, MolSA, SASA, and PSA were analyzed for ABL1 kinase complexes with co-crystallized dasatinib and derivatives 45375848, 88575518, and 23589024 (**Fig. S4**). Ligand RMSD measured the deviation from the reference conformation, while rGyr assessed ligand compactness. All parameters were within the expected range, confirming ligand stability throughout the simulation.

DFT studies

Density functional theory (DFT) calculations, like molecular docking and simulation studies, have become routinely used tools in drug discovery programs [36]. A plethora of research available shows that DFT can be used in drug modelling [29], designing polymer-based drug delivery [37], and calculating drug numerous other molecular and quantum descriptors [29]. In the present study, we also computed the energy and distribution of frontiers molecular orbitals, which were then used to estimate the molecular chemical indexes like chemical reactivity, hardness, softness, etc. In dasatinib and **23589024**, the highest occupied molecular orbital (HOMO) was located over N-(2-chloro-6-methylphenyl)-2-(methylamino)thiazole-5-carboxamide fragment. On the other hand, it was over thiazole and quinazoline cores in **45375848** and **45375848**. LUMO was found to be over pyridine or pyrimidine fragments of the molecule (**Fig. 8**). The HOMO-LUMO gap (ΔE), which is a key indicator of a molecule's chemical stability and reactivity, was found to be higher as compared to the earlier studied small molecules. Also it was

noted that the ΔE was relatively higher for Dasatinib (ΔE = 4.47 eV) than the screened compounds (ΔE = 4.10-4.39 eV).

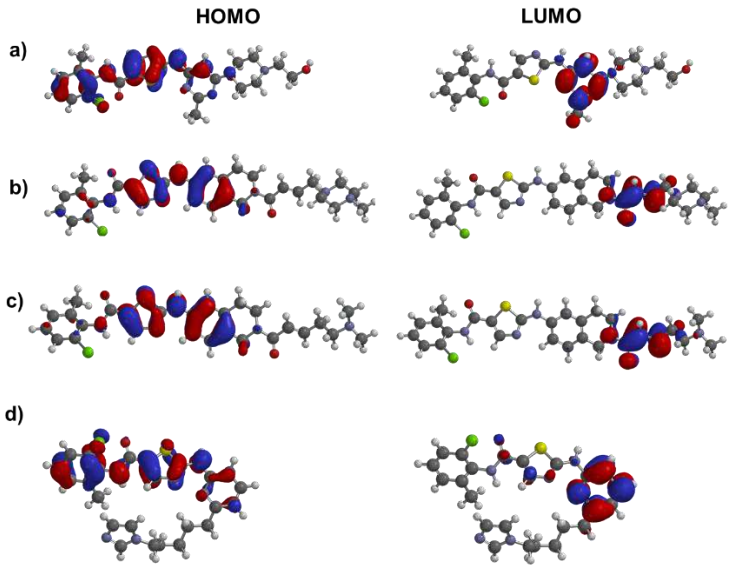

Figure 8: Chemical structures of dasatinib, 45375848, 45375848, and 23589024 (a-d, respectively)**.** Highlighted areas show common fragments.

Table 3. Chemical reactivity parameters were calculated by density functional theory (DFT)/B3LYP (Becke's three-parameter hybrid exchange functional with the Lee–Yang–Parr correlation functional) method with a polarisation basis set 6-31G* in the gas phase.

Code #	E_{HOMO} (eV)	E_{LUMO} (eV)	ΔE^a (eV)	I^b (eV)	A^c (eV)	χ^d (eV)	η^e (eV)	σ^f (eV^{-1})	μ^g (eV)	ω^h (eV)
dastanib	–5.91	–1.44	4.47	5.91	1.44	3.67	2.24	0.11	–3.67	3.01
45375848	–5.62	–1.52	4.10	5.62	1.52	3.57	2.05	0.12	–3.57	3.10
88575518	–5.62	–1.49	4.13	5.62	1.49	3.55	2.06	0.12	–3.55	3.05
23589024	–5.80	–1.41	4.39	5.80	1.41	3.60	2.20	0.11	–3.60	2.95

a = $\left| E_{HOMO} - E_{LUMO} \right|$; b = − E_{HOMO}; c = − E_{LUMO}; d = (I + A)/2; e = (I − A)/2; f = 1/2η; g = -(I + A)/2; h = $\mu^2/2\eta$

Conclusion

ABL1 is an important protein that helps control many critical cell functions, such as cell movement, attachment, and the ability to repair DNA. Through its involvement in these essential processes, ABL1 contributes to maintaining normal cell function, growth, and survival. Dysregulation of ABL1 is associated with several diseases, including CML, highlighting its importance as a therapeutic target. This study explored the potential of dasatinib and its derivatives as inhibitors of ABL1 was explored through a series of computational techniques, including molecular docking, ADMET analysis, DFT calculations, and MD simulations. The docking studies revealed that three ligands, 45375848, 88575518, and 23589024, demonstrated strong binding affinities, with docking energies indicating favourable interactions with the ABL1 receptor. Additionally, as assessed by ADMET analysis, these ligands exhibited promising drug-like properties and were able to stabilize the receptor's structure, as shown in the MD simulations. These results suggest that the shortlisted compounds have the potential to serve as effective ABL1 inhibitors, offering a strong foundation for future research. Further in vivo and in vitro studies are warranted to evaluate the therapeutic potential and efficacy of these compounds in treating diseases associated with ABL1 dysregulation, particularly in cancer. Given the central role of ABL1 in cellular signaling and disease progression, these compounds could provide valuable insights into the development of targeted therapies.

Author Contributions

All listed authors have significantly contributed to the work through direct intellectual input and have given their approval for its publication.

Acknowledgements

This research has been funded by Scientific Research Deanship at University of Ha'il - Saudi Arabia through project number <<RG-24 095>>.

Conflict of interest

The authors declare that the research was conducted in the absence of any commercial or financial relationships that could be construed as a potential conflict of interest.

SUPPLEMENTARY MATERIAL

The Supplementary Material for this article can be found online at: Supplementary data.docx.

Reference

1. Bray, F., Laversanne, M., Sung, H., Ferlay, J., Siegel, R. L., Soerjomataram, I., et al. (2024). Global cancer statistics 2022: GLOBOCAN estimates of incidence and mortality worldwide for 36 cancers in 185 countries. *CA: a cancer journal for clinicians, 74*(3), 229-263. https://doi.org/10.3322/caac.21834

2. Vasan, N., Baselga, J., & Hyman, D. M. (2019). A view on drug resistance in cancer. *Nature, 575*(7782), 299-309. https://doi.org/10.1038/s41586-019-1730-1

3. Khatri, A., Wang, J., & Pendergast, A. M. (2016). Multifunctional Abl kinases in health and disease. *Journal of cell science, 129*(1), 9-16. https://doi.org/10.1242/jcs.175521

4. Khatri, A. (2018). *The Role of Abl Kinases in Lung Injury and Cancer*. Duke University,

5. Tanim, M. T. H., Nath, S. D., Khan, S. F., Khan, A., & Sajib, A. A. (2024). Transcriptomes of cervical cancer provide novel insights into dysregulated pathways, potential therapeutic targets, and repurposed drugs. *Cancer Treatment and Research Communications, 39*, 100808. https://doi.org/10.1016/j.ctarc.2024.100808

6. Dasgupta, Y., Koptyra, M., Hoser, G., Kantekure, K., Roy, D., Gornicka, B., et al. (2016). Normal ABL1 is a tumor suppressor and therapeutic target in human and mouse leukemias expressing oncogenic ABL1 kinases. *Blood, The Journal of the American Society of Hematology, 127*(17), 2131-2143. https://doi.org/10.1182/blood-2015-11-681171

7. Colicelli, J. (2010). ABL tyrosine kinases: evolution of function, regulation, and specificity. *Science signaling, 3*(139), re6-re6. https://doi.org/10.1126/scisignal.3139re6

8. Lee, B. J. (2016). *Mechanisms of Tyrosine Kinase Activation and Drug Response in Chronic and Acute Myeloid Leukemias*. UCSF,

9. Quintás-Cardama, A., & Cortes, J. (2009). Molecular biology of bcr-abl1–positive chronic myeloid leukemia. *Blood, The Journal of the American Society of Hematology, 113*(8), 1619-1630. https://doi.org/10.1182/blood-2008-03-144790

10. Greuber, E. K., Smith-Pearson, P., Wang, J., & Pendergast, A. M. (2013). Role of ABL family kinases in cancer: from leukaemia to solid tumours. *Nature Reviews Cancer, 13*(8), 559-571. https://doi.org/10.1038/nrc3563

11. Poudel, G., Tolland, M. G., Hughes, T. P., & Pagani, I. S. (2022). Mechanisms of resistance and implications for treatment strategies in chronic myeloid leukaemia. *Cancers, 14*(14), 3300. https://doi.org/10.3390/cancers14143300

12. Masai, H., Terao, J., Makuta, S., Tachibana, Y., Fujihara, T., & Tsuji, Y. (2014). Enhancement of Phosphorescence and Unimolecular Behavior in the Solid State by Perfect Insulation of Platinum–Acetylide Polymers. *Journal of the American Chemical Society, 136*(42), 14714-14717. https://doi.org/10.1021/ja508636z

13. Redaelli, S., Mologni, L., Rostagno, R., Piazza, R., Magistroni, V., Ceccon, M., et al. (2012). Three novel patient-derived BCR/ABL mutants show different sensitivity to second and third generation tyrosine kinase inhibitors. *American journal of hematology, 87*(11), E125. https://doi.org/10.1002/ajh.23338

14. Tan, K.-W., Zhu, Y.-Y., Qiu, Q.-C., Wang, M., Shen, H.-J., Huang, S.-M., et al. (2023). Rapid molecular response to dasatinib in Ph-like acute lymphoblastic leukemia patients with ABL1 rearrangements: case series and literature review. *Annals of Hematology, 102*(9), 2397-2402. https://doi.org/10.1007/s00277-023-05236-z

15. Yeung, D., Moulton, D., Heatley, S., Nievergall, E., Dang, P., Braley, J., et al. (2015). Relapse of BCR-ABL1-like ALL mediated by the ABL1 kinase domain mutation T315I following initial response to dasatinib treatment. *Leukemia, 29*(1), 230-232. https://doi.org/10.1038/leu.2014.256
16. Conchon, M., Freitas, C. M. B. d. M., Rego, M. A. d. C., & Braga Junior, J. W. R. (2011). Dasatinib: clinical trials and management of adverse events in imatinib resistant/intolerant chronic myeloid leukemia. *Revista brasileira de hematologia e hemoterapia, 33*, 131-139. https://doi.org/10.5581/1516-8484.20110034
17. Kim, S., Chen, J., Cheng, T., Gindulyte, A., He, J., He, S., et al. (2023). PubChem 2023 update. *Nucleic acids research, 51*(D1), D1373-D1380. https://doi.org/10.1093/nar/gkac956
18. Tokarski, J. S., Newitt, J. A., Chang, C. Y. J., Cheng, J. D., Wittekind, M., Kiefer, S. E., et al. (2006). The structure of Dasatinib (BMS-354825) bound to activated ABL kinase domain elucidates its inhibitory activity against imatinib-resistant ABL mutants. *Cancer research, 66*(11), 5790-5797. https://doi.org/10.1158/0008-5472.CAN-05-4187
19. Johnston, R. C., Yao, K., Kaplan, Z., Chelliah, M., Leswing, K., Seekins, S., et al. (2023). Epik: p K a and Protonation State Prediction through Machine Learning. *Journal of chemical theory and computation, 19*(8), 2380-2388. https://doi.org/10.1021/acs.jctc.3c00044
20. Friesner, R. A., Murphy, R. B., Repasky, M. P., Frye, L. L., Greenwood, J. R., Halgren, T. A., et al. (2006). Extra precision glide: Docking and scoring incorporating a model of hydrophobic enclosure for protein− ligand complexes. *Journal of medicinal chemistry, 49*(21), 6177-6196. https://doi.org/10.1021/jm051256o
21. van Zundert, G. C., Moriarty, N. W., Sobolev, O. V., Adams, P. D., & Borrelli, K. W. (2021). Macromolecular refinement of X-ray and cryoelectron microscopy structures with Phenix/OPLS3e for improved structure and ligand quality. *Structure, 29*(8), 913-921. e914. https://doi.org/10.1016/j.str.2021.03.011
22. Miller, E. B., Murphy, R. B., Sindhikara, D., Borrelli, K. W., Grisewood, M. J., Ranalli, F., et al. (2021). Reliable and accurate solution to the induced fit docking problem for protein–ligand binding. *Journal of chemical theory and computation, 17*(4), 2630-2639. https://doi.org/10.1021/acs.jctc.1c00136
23. Sherman, W., Day, T., Jacobson, M. P., Friesner, R. A., & Farid, R. (2006). Novel procedure for modeling ligand/receptor induced fit effects. *Journal of medicinal chemistry, 49*(2), 534-553. https://doi.org/10.1021/jm050540c
24. Haque, A., Alenezi, K. M., Khan, M. W. A., Soury, R., Khan, M. S., Ahamad, S., et al. (2023). In silico evaluation of 4-thiazolidinone-based inhibitors against the receptor for advanced glycation end products (RAGE). *Journal of Biomolecular Structure and Dynamics*, 1-12. https://doi.org/10.1080/07391102.2023.2290621
25. Bowers, K. J., Chow, E., Xu, H., Dror, R. O., Eastwood, M. P., Gregersen, B. A., et al. Scalable algorithms for molecular dynamics simulations on commodity clusters. In *Proceedings of the 2006 ACM/IEEE Conference on Supercomputing, 2006* (pp. 84-es)
26. Shivakumar, D., Williams, J., Wu, Y., Damm, W., Shelley, J., & Sherman, W. (2010). Prediction of absolute solvation free energies using molecular dynamics free energy perturbation and the OPLS force field. *Journal of chemical theory and computation, 6*(5), 1509-1519. https://doi.org/10.1021/ct900587b

27. Pandrala, M., Bruyneel, A. A. N., Hnatiuk, A. P., Mercola, M., & Malhotra, S. V. (2022). Designing novel BCR-ABL inhibitors for chronic myeloid leukemia with improved cardiac safety. *Journal of medicinal chemistry, 65*(16), 10898-10919. https://doi.org/10.1021/acs.jmedchem.1c01853
28. Zhou, T., Commodore, L., Huang, W. S., Wang, Y., Thomas, M., Keats, J., et al. (2011). Structural mechanism of the pan-BCR-ABL inhibitor ponatinib (AP24534): lessons for overcoming kinase inhibitor resistance. *Chemical biology & drug design, 77*(1), 1-11. https://doi.org/10.1111/j.1747-0285.2010.01054.x
29. Arias, F., Franco-Montalban, F., Romero, M., Carrión, M. D., & Camacho, M. E. (2021). Synthesis, bioevaluation and docking studies of new imidamide derivatives as nitric oxide synthase inhibitors. *Bioorganic & Medicinal Chemistry, 44*, 116294. https://doi.org/10.1016/j.bmc.2021.116294
30. Shahbazi, S., Kaur, J., Singh, S., Achary, K. G., Wani, S., Jema, S., et al. (2018). Impact of novel N-aryl piperamide NO donors on NF-κB translocation in neuroinflammation: rational drug-designing synthesis and biological evaluation. *Innate Immunity, 24*(1), 24-39. https://doi.org/10.1177/1753425917740727
31. Hollingsworth, S. A., & Dror, R. O. (2018). Molecular dynamics simulation for all. *Neuron, 99*(6), 1129-1143. https://doi.org/10.1016/j.neuron.2018.08.011
32. Celik, L., Lund, J. D. D., & Schiøtt, B. (2007). Conformational dynamics of the estrogen receptor α: molecular dynamics simulations of the influence of binding site structure on protein dynamics. *Biochemistry, 46*(7), 1743-1758. https://doi.org/10.1021/bi061656t
33. Spyrakis, F., BidonChanal, A., Barril, X., & Javier Luque, F. (2011). Protein flexibility and ligand recognition: challenges for molecular modeling. *Current topics in medicinal chemistry, 11*(2), 192-210. https://doi.org/10.2174/156802611794863571
34. Kumar, S., Sharma, P. P., Shankar, U., Kumar, D., Joshi, S. K., Pena, L., et al. (2020). Discovery of new hydroxyethylamine analogs against 3CLpro protein target of SARS-CoV-2: Molecular docking, molecular dynamics simulation, and structure–activity relationship studies. *Journal of chemical information and modeling, 60*(12), 5754-5770. https://doi.org/10.1021/acs.jcim.0c00326
35. Lecina, D., Gilabert, J. F., & Guallar, V. (2017). Adaptive simulations, towards interactive protein-ligand modeling. *Scientific reports, 7*(1), 8466. https://doi.org/10.1038/s41598-017-08445-5
36. Sabe, V. T., Ntombela, T., Jhamba, L. A., Maguire, G. E., Govender, T., Naicker, T., et al. (2021). Current trends in computer aided drug design and a highlight of drugs discovered via computational techniques: A review. *European Journal of Medicinal Chemistry, 224*, 113705. https://doi.org/10.1016/j.ejmech.2021.113705
37. Adekoya, O. C., Adekoya, G. J., Sadiku, E. R., Hamam, Y., & Ray, S. S. (2022). Application of DFT calculations in designing polymer-based drug delivery systems: An overview. *Pharmaceutics, 14*(9), 1972. https://doi.org/10.3390/pharmaceutics14091972